Faraday Discussions

Accepted Manuscript

Faraday Discussions

Royal Society of Chemistry

ROYAL SOCIETY OF CHEMISTRY

www.rsc.org/faraday_d

Spatio-Temporal Correlations in Aqueous Systems: Computational Studies of Static and Dynamic Heterogeneity by 2D-IR Spectroscopy

Rikhia Ghosh, Tuhin Samanta, Saikat Banaerjee, Rajib Biswas and Biman Bagchi[*]

SSCU, Indian Institute of Science, Bangalore 560012, India

Abstract

Local heterogeneity is ubiquitous in natural aqueous systems. It can be caused locally by external biomolecular subsystems like proteins, DNA, micelles and reverse micelles, nanoscopic materials etc. but can also be intrinsic to the thermodynamic nature of the aqueous solution itself (like binary mixtures or at gas-liquid interface). The altered dynamics of water in presence of such diverse surfaces have attracted considerable attention in recent years. As these interfaces are quite narrow, only a few molecular layers thick, they are hard to study by conventional methods. Recent development of two dimensional infra-red (2D-IR) spectroscopy allows us to estimate length and time scales of such dynamics fairly accurately. In this work, we present a series of interesting studies employing two dimensional infra-red spectroscopy (2D-IR) to investigate (i) heterogeneous dynamics of water inside reverse micelles of varying sizes, (ii) supercritical water near the Widom line that is known to exhibit pronounced density fluctuations and also study (iii) collective and local polarization fluctuation of water molecules in presence of several different proteins. Spatio-temporal correlation of confined water molecules with varying size of reverse micelles is well captured through the spectral diffusion of corresponding 2D-IR spectra. In the case of supercritical water also, we observe strong signature of dynamic heterogeneity from the elongated nature of the 2D-IR spectra. In this case the relaxation is ultrafast. We find remarkable agreement between different tools employed to study the relaxation of density heterogeneity. For aqueous protein solutions, we find that the calculated dielectric constant of the respective systems unanimously show a noticeable increment compared to that of neat water. However, 'effective' dielectric constant for successive layers shows significant variation, with the layer adjacent to protein having much lower value. Relaxation is also slowest at the surface. We find that the dielectric constant achieves bulk value at distances more than 3 nm from the surface of the protein.

I. Introduction

Understanding structure and dynamics of water molecules, in bulk as well as in aqueous solutions of biomolecules (proteins, DNA, lipids) have been subjects of continuing interest for many decades[1-10]. A common characteristic of these systems is found to be the appearance of a local heterogeneity in the liquid near the interface that may propagate only up to 5-10 molecular layers (that is, 2-4 nm)[11]. Existence of heterogeneity at such small length scale make interfacial water a difficult system to study by using conventional techniques, such as light and neutron scattering, nuclear magnetic resonance (NMR) or linear spectroscopic methods like Raman linewidth measurements. Since the heterogeneity is found to be dynamic in nature, associated with ultrafast time scales in many of the cases, even x-ray scattering or electron microscopic techniques are not too useful.

Fortunately recently developed two dimensional infra-red spectroscopy (2D-IR) can serve as a powerful technique for measuring the water dynamics with its femtosecond time resolution[12,13]. In 2D-IR spectroscopy[14], one can use the –O-H stretching frequency of water, or some other molecule, as a reliable marker of the position of the molecule. The –O-H stretching frequency in water is known to undergo large variation[15]. For example, those water molecules which are hydrogen bonded to a charged group at the inner surface or reverse micelle, the –O-H stretching frequency can be as low as 2800 cm^{-1} while the corresponding value in bulk is ~ 3600 cm^{-1}. 2D-IR spectroscopy thus provides a valuable method to obtain spatio-temporal resolution that is not achievable by other conventional methods. Water dynamics at the interface of biomolecules can also be explored through dielectric relaxation measurements, albeit with much poorer spatial resolution.

Water at the surface of biological macromolecules, such as proteins, DNA and at extended biological surfaces such as lipid bilayers, is now known as biological water[4,9,16-18]. Many of the characteristics of water at such surfaces are markedly different from those of bulk water, marked by lower values of an effective dielectric constant, slower dynamical responses and higher density. In fact, proper hydration of proteins and enzymes is predominantly important for the stability of the structure as well as functionality at the specified site. This explains the largely growing attention to understand the underlying characteristics of biological water. Dielectric spectra of aqueous protein solutions have been thoroughly studied for more than 60 years. However, the effect of large dipole moments of proteins on polarization fluctuation of the aqueous solution has still not been adequately addressed.

In this work, we employ 2D-IR spectroscopy to quantitatively measure the nature of water dynamics (i) inside reverse micelle and (ii) in supercritical water. (iii) We also explore heterogeneity of water at biomolecular interface, selectively measuring polarization fluctuation of water for aqueous protein solutions. To understand the altered dynamics of water we perform a layer wise decomposition of water inside reverse micelle, with an aim to enumerate the relative contributions of different layers water molecules to the calculated 2D-IR spectrum. We further quantify the variation of static and dynamic heterogeneity in super critical water across the Widom line is studied by constructing the 2D-IR spectrum of the '-O-H' stretch as well as from non-linear density response function, $\chi_4(t)$ and non-Gaussian parameter $\alpha_2(t)$. All the variables beautifully capture the ultrafast time scale of heterogeneity prevalent near the Widom line.

Next we carry out a systematic study of the polarization fluctuation by considering two proteins immunoglobin binding domain protein G (GB1), lysozyme (Lys) immersed in a large number of water molecules. Analysis of the total and local polarization fluctuation show surprisingly different water dynamics for the two proteins.

In this report, we have attempted to bring together three different types of aqueous systems, by using mostly 2D-IR spectroscopic technique, described in section II. e For two of them, discussed in sections III and IV, we could construct 2D-IR spectra, and study heterogeneous dynamics through anisotropy. In the third case, discussed in section V, we study spatio-temporal correlation in polarization fluctuations.

II. Spectroscopic Modeling of 2D-IR

The experimentally observed 2D-IR response functions $R_{l,m,n}$ are successfully obtained theoretically from the line shape function $g(t)$ as follows[14]

$$R_{1,2,3} = i\mu_{01}^4 \left(e^{-i\omega_{01}(t_3-t_1)} - e^{-i\left((\omega_{01}-\Delta)t_3 - \omega_{01}t_1\right)} \right)$$
$$e^{-g(t_1)+g(t_2)-g(t_3)-g(t_1+t_2)-g(t_2+t_3)+g(t_1+t_2+t_3)}$$

(1)

$$R_{4,5,6} = i\mu_{01}^4 \left(e^{-i\omega_{01}(t_3+t_1)} - e^{-i\left((\omega_{01}-\Delta)t_3 + \omega_{01}t_1\right)} \right)$$
$$e^{-g(t_1)-g(t_2)-g(t_3)+g(t_1+t_2)+g(t_2+t_3)-g(t_1+t_2+t_3)}$$

(2)

Where $\mathbf{\mu}_{10}$ is the 1-0 matrix element of the dipole operator and $\omega_{10}(t)$ is the classical time dependent transition frequency. $g(t)$ is the corresponding lineshape function that is obtained

4

analytically from Kubo's lineshape theorem using the frequency fluctuation correlation function

(FFCF) $c(t) = \langle \delta\omega(t)\delta\omega(0) \rangle$. The exact form of $g(t)$ is given by the following expression,

$$g(t) = \int_0^t d\tau' \int^{\tau'} \langle \delta\omega(\tau'')\delta\omega(0) \rangle d\tau'' \tag{3}$$

All the response functions are Fourier transformed to reveal purely absorptive 2D IR spectra.

Equations (2) employ Condon approximation. It has been shown that non-Condon effects are significant for –O-H vibrational mode of water. We are currently investigating such non-Condon effects. Results presented here, however, use Eq.2, and therefore, are only semi-quantitatively reliable. However, some of the results are quite striking and we expect them to capture much of the true behavior.

III.   Reverse Micelles : From Spectra Resolution to Spatial Decomposition
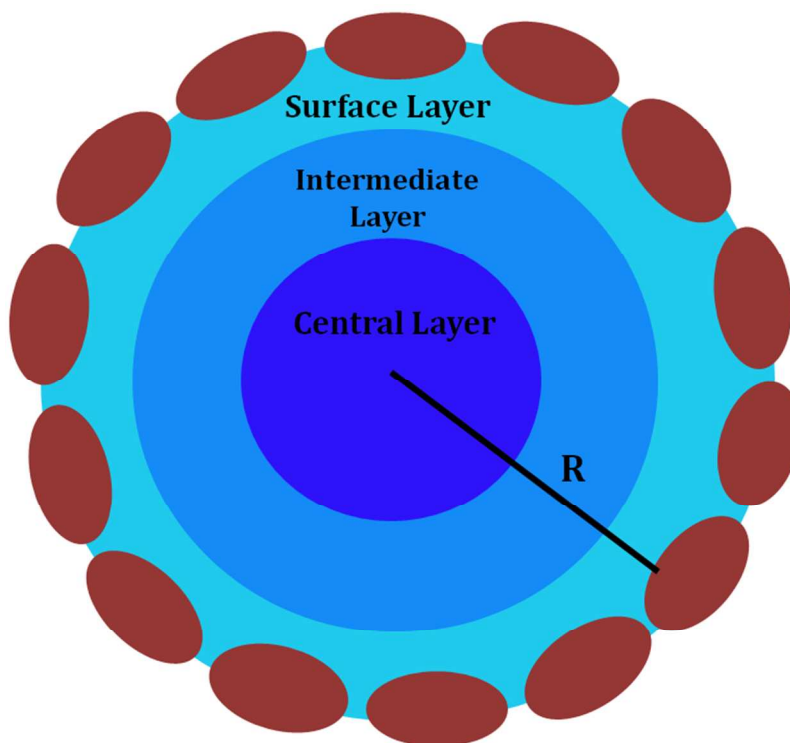
Figure 1. Schematic diagram showing layering of water inside a representative reverse micelle of effective radius R.

As mentioned earlier, reverse micelles (RM) provide us with unique opportunity to study the ability of 2D-IR spectroscopy to explore the length and time scales of local heterogeneity. Here we adopt a two fold approach. First, we carry out detail simulations to obtain microscopic details. Second, we use the simulation trajectories to construct the 2D-IR spectrum where water molecules are selected from different layers from the surface. The comparison between the two allows us to use spectral resolution available from 2D-IR spectroscopy to a spatial decomposition of structure and dynamics.

A. Simulation details

We use united atom description for Isooctane and all atom description for the surfactant and water molecules. We use TIP4P-2005 water like molecules[19]. The united atom description of Isooctane is obtained from GROMOS53A6 force field. The initial spherical RMs structures are prepared using packmol and then solvated with Isooctane like molecules in a cubic box. We use GROMACS, version 4.5.5[20] for all the MD simulations in this study. Steepest descent method is used for energy minimization of the initial configuration; followed by position restrained simulation in the isothermal isobaric ensemble (constant pressure, NPT) for 2ns, by imposing position restrain condition on oxygen of water and sulfur of AOT. We use fourth order Particle Mesh Ewald (PME) summation for long range interaction with grid spacing of 0.16. We equilibrate the system initially in NPT ensemble for 10 ns followed by 10 ns in the canonical ensemble (constant volume, NVT). Finally data acquisitions are performed in NVT ensemble. The system is maintained at constant temperature of 300 K and 1 atm pressure by using Nosé-Hoover thermostat[21,22] and Parrinello-Rahman barostat[23]. Periodic boundary conditions are applied in all three directions. The details of different RMs constituents are summarized in **Table 1** (size index is given as w_0, which is the number of water molecules per surfactant molecule).

Table 1: Compositions of simulated RMs

w_0	n_{H_2O}	n_{AOT}/n_{Na}	n_{ISO}
2.0	52	26	504
4.0	140	35	930
7.5	525	70	1138
10.0	980	98	1377

We calculate bulk properties by taking 1000 TIP4P-2005 water molecules in a cubic box.

B. Evolution of water dynamics with increasing size of reverse micelle: 2D-IR spectroscopic view of heterogeneity

Water dynamics inside reverse micelles of varying sizes is a striking example of heterogeneous spatio-temporal correlations. We explore these aspects by considering reverse micelles of different sizes into different number of layers based on the radial density distribution of water. The layer-wise classifications of water in the RMs based on the radial density distribution of water are summarized in **Table 2**.

From the radial density distributions of water from surface to center of reverse micelle, we conclude the existence of distinct layering of water molecules (schematic diagram shown in **Figure 1**). In the case of the lowest RM size i.e. $w_0 = 2.0$, it is observed that almost all water molecules are restricted in the vicinity of surface head groups of AOT molecules, forming a single water layer. However, with increasing RM size presence of three distinct layers of water is observed, based on structural and dynamical properties. The water molecules bound to the surface head groups of AOT are named as *surface layer* (SL); subsequent to the SL there is an intermediate *water* (IL) layer followed by the *central water pool* (CL).

Table – 2: Layer-wise classification of water in the reverse micelle based on the radial density distribution of water. Distance from sulfur atom of AOT is denoted as r, and $\overline{n}_{H_2O}$ is the average number of water molecules present in different layers. For $w_0 = 2.0$ all AOT head groups are not solvated by water, which led us to assume a single water layer in this RM.

Reverse Micelles	Surface Layer (SL)		Intermediate Layer (IL)		Central Layer (CL)	
	r (Å)	$\overline{n}_{H_2O}$	r (Å)	$\overline{n}_{H_2O}$	r (Å)	$\overline{n}_{H_2O}$
$w_0 = 4.0$	r ≤ 4.96Å	111	r > 4.96Å	29	-	-
$w_0 = 7.5$	r ≤ 5.0 Å	332	5.0Å ≥ r > 5.9Å	72	r > 5.9Å	121

| $w_0 = 10.0$ | $r \le 5.0$ Å | 474 | 5.0Å $\ge$ r >6.9Å | 269 | r >6.9Å | 237 |

Next we calculate layerwise hydrogen bond dynamics of water for reverse micelles of different sizes by evaluating the corresponding frequency fluctuation correlation functions (FFCF) of all the –O-H bonds. FFCF efficiently evaluates the spectral diffusion in terms of time scales of the dynamics. Layer wise decomposition of FFCF gives rise to the following equation

$$\langle \delta\omega(t)\delta\omega(0)\rangle = \frac{1}{N_L}\sum_{L=1}^{N_L}\frac{1}{N_W^{LL}}\sum_{i=1}^{N_W^{LL}}\left[\langle\delta\omega_i^L(t)\delta\omega_i^L(0)\rangle\right]$$
$$+\frac{1}{N_L(N_L-1)}\sum_{L_1=1}^{N_L}\sum_{L_2=1}^{N_L}\frac{\delta_{L_1 L_2}}{N_W^{L_1 L_2}}\sum_{i=1}^{N_W^{L_1 L_2}}\left[\langle\delta\omega_i^{L_1}(t)\delta\omega_i^{L_2}(0)\rangle\right] \tag{4}$$

where $\delta\omega_i^L$ is the frequency fluctuation of O-H bond of i-th water molecule staying in layer L, N_L is the total number of layers, N_W^{LL} is the number of water molecules present in layer L throughout the detection time and give the self-term $\langle\delta\omega_i^L(t)\delta\omega_i^L(0)\rangle$, similarly $N_W^{L_1 L_2}$ is the total number of water molecules which give the cross term $\langle\delta\omega_i^{L_1}(t)\delta\omega_i^{L_2}(0)\rangle$, $\delta_{L_1 L_2}$ has a value 0 if $L_1 = L_2$ and else 1.0. We compute the self-term of FFCF using the layer definition. The layer wise calculation of FFCFs (shown in supporting information **Figure S1**) reveals clear distinction of hydrogen bond dynamics in different reverse micelles.

To extract the corresponding 2D-IR spectra, we use the following fitting function to fit the FFCFs,

$$c(t) = a_1\cos(\omega_{OO}t)e^{-t/\tau_1} + a_2 e^{-t/\tau_2} + a_3 e^{-t/\tau_3} \tag{5}$$

Using the fitting parameters we calculate the lineshape function $g(t)$, and finally we obtain the 2D IR spectra from the corresponding response functions as described in Eq. (1) and Eq. (2). 2D

IR spectra of different layers of reverse micelles as well as that of bulk are shown in **Figure 2**, obtained using waiting time 500 fs.
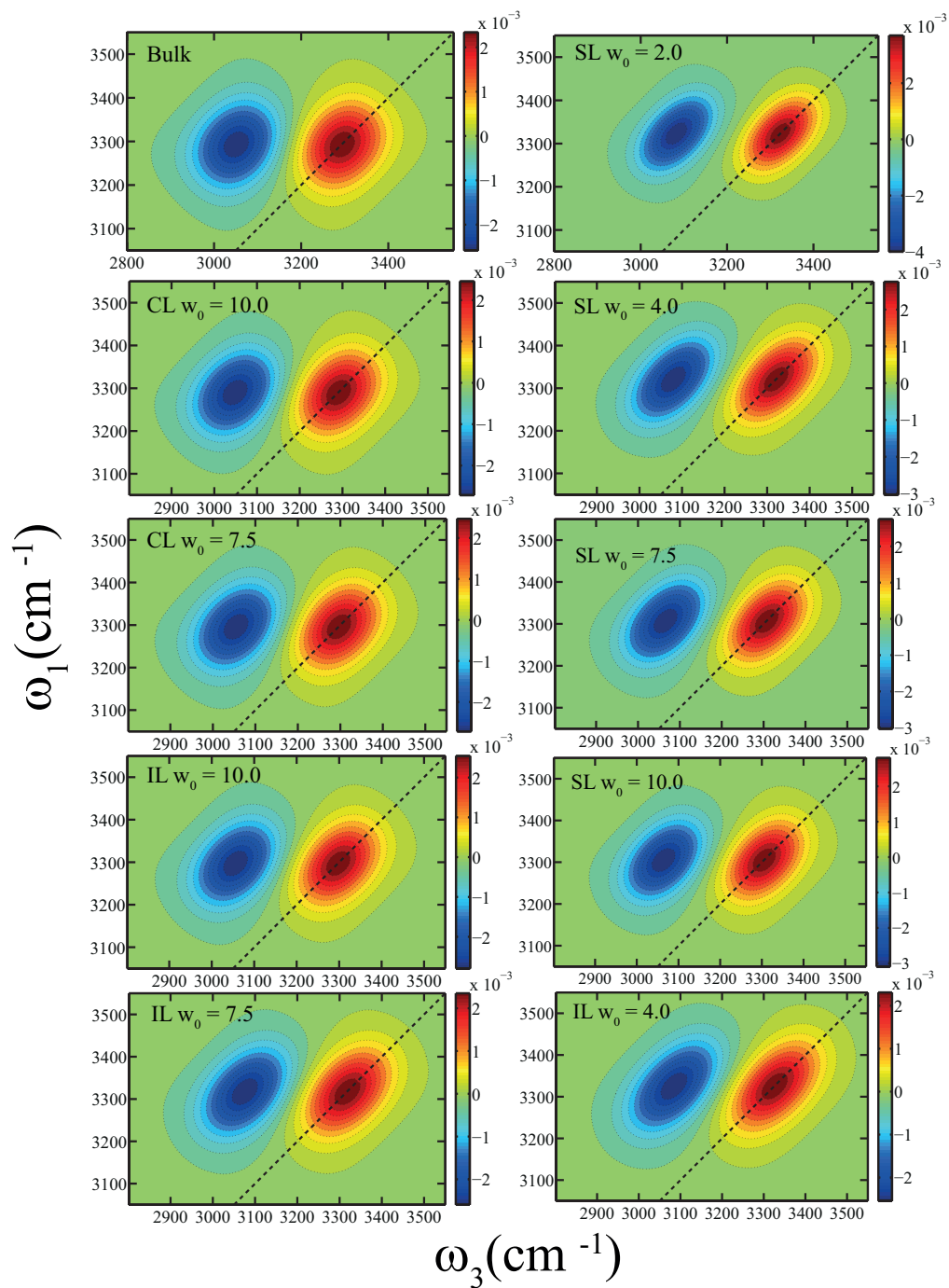
Figure 2. The 2D IR spectra of O-H stretch in bulk water and in different layers of reverse micelles (presented clockwise starting from the one for bulk water). Here the layer-wise 2D IR spectrum is calculated by tagging the water molecules which stay continuously in that layer during the data acquisition. All the spectra are obtained at waiting time of 500 fs. The shape of the spectrum depends on two factors: the size of the reverse micelles and the position of the layer we are looking at. It is clear from the figures that as reverse micelle size increases the spectrum become more bulk like in the central layer.

The red bands arise from the $0 \rightarrow 1$ vibrational transition whereas the blue bands arise from the vibrational echo emission at $1 \rightarrow 2$ vibrational frequency. The spectra of $0 \rightarrow 1$ transition clearly show substantial elongation along the diagonal for surface water layer (SL) with increasing reverse micelle size which is a measure of increasing inhomogeneity. In case of subsequent intermediate layers (IL) also, considerable heterogeneity is prevalent, as can be seen from elongated $0 \rightarrow 1$ transition spectra. However the central layers (CL) for the corresponding reverse micelles are found to be showing bulk-like behavior. The altered dynamics of water with increasing reverse micelle size serves as a powerful example of spatio-temporal correlation of heterogeneous water dynamics.
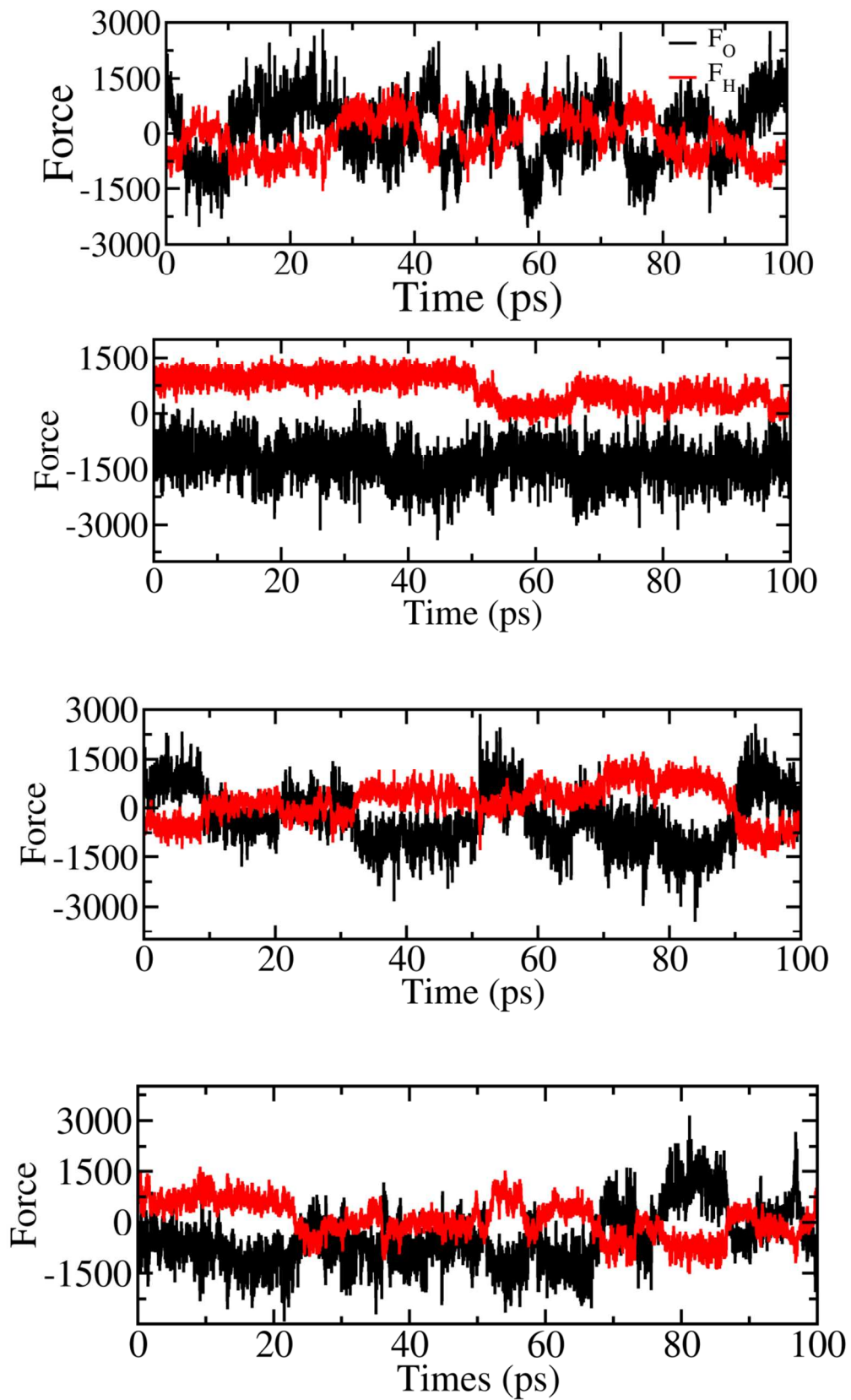
Figure 3. Force trajectories (projected force in unit of KJ mol^{-1} nm^{-1}) acting separately on oxygen atom (in black) and hydrogen atom (in red) of water in case of (a) bulk water (b) tagged surface water of reverse micelle size $w_0 = 2.0$ (c) tagged water in the intermediate layer of reverse micelle size $w_0 = 4.0$ (d) tagged central water molecule of reverse micelle size $w_0 = 10.0$.

It is broadly acknowledged that anti-correlation existing between forces on oxygen and hydrogen atom of –O-H bonds plays an important role for the decay of FFCFs[24]. Bulk water is found to exhibit ultrafast decay of FFCF, which essentially arises due to large amplitude angular jumps of water molecules and appearance of large cross correlation of projected force on oxygen and hydrogen atoms of the –O-H bonds. We find such evidences from the corresponding force trajectories (**Figure 3**). It can be seen that surface effect significantly reduces anti-correlation between forces on oxygen and hydrogen. However substantial anti-correlation is prevalent at the center of larger reverse micelles (Figure 3(c)) which eventually reflects the faster decay of FFCF in this case (as can be seen in **Figure S1**)

IV.   Enhanced heterogeneity of supercritical water across the Widom line
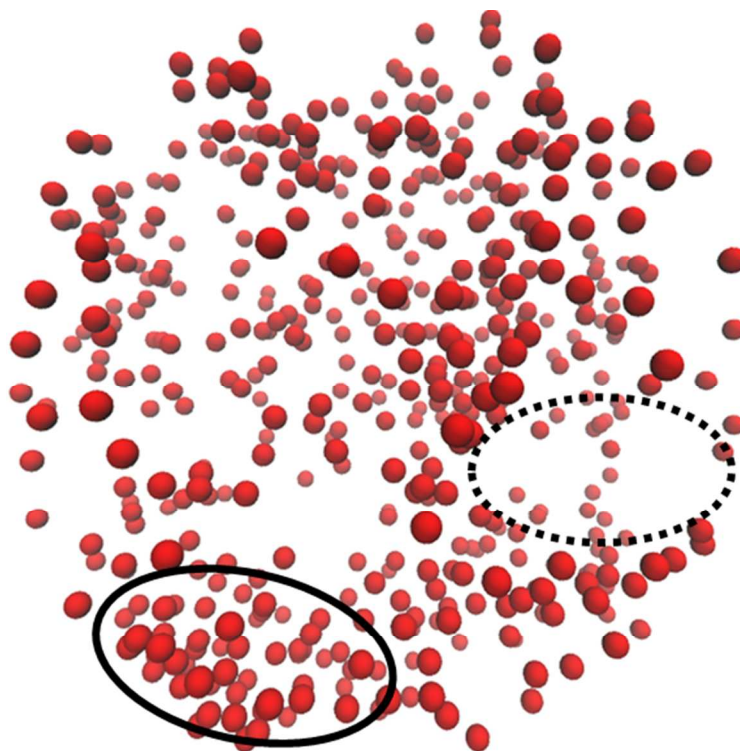
Figure 4. Representative snapshot of supercritical water. Prominent signature of co-existing high density region (shown by solid circle) and low density region (marked by dashed circle) is found here.

The upward line that originates at the critical temperature (T_C) and separates (in the temperature-pressure-density plane) a gas-like region from a liquid-like region above T_C, is known as the Widom line. The critical point of real water is located at pressure (P_c) 220.55 bar, temperature (T_c) of 647.13 K and density (ρ_c) 0.322 gm/cm^3. SCW is believed to exist at temperatures above 647.13 K. Because of the proximity to critical point, SCW exhibit properties of both liquid and gas in a combined manner (representative snapshot provided in **Figure 4**). In our work we use SPC/E water model whose critical parameters are $T_c = 651.7$ K, $\rho_c = 0.326$ g/cm^3, and $P_c = 189$ bar. These values are very close to the experimental gas-liquid coexistence point.

Although the fluid here is macroscopically homogeneous, supercritical water (SCW) near the Widom line is known to exhibit pronounced density fluctuations, remnant of critical phenomena.

Variation of static and dynamic heterogeneity in SCW across the Widom line is studied (i) by constructing the 2D-IR spectrum of the '-O-H' stretch (ii) from non-linear density response function, $\chi_4(t)$ and (iii) non-Gaussian parameter $\alpha_2(t)$. All of them show sudden and sharp change close to the Widom line.

A. Simulation Details

All the simulations for supercritical water are carried out using 2048 SPC/E water in a cubic box. Similar steps of equilibration, as that for water inside reverse micelle, are followed in this case also. The temperature is kept constant at 670K using Nose-Hoover thermostat[21,22] the pressure is kept at 217.3 atm. Density is varied consistently along the Widom line keeping the temperature constant (ρ 0.32, 0.33 and 0.34 gm/cm^3 respectively).

B. 2D-IR spectroscopic study of supercritical water: Evidence of static and dynamic heterogeneity
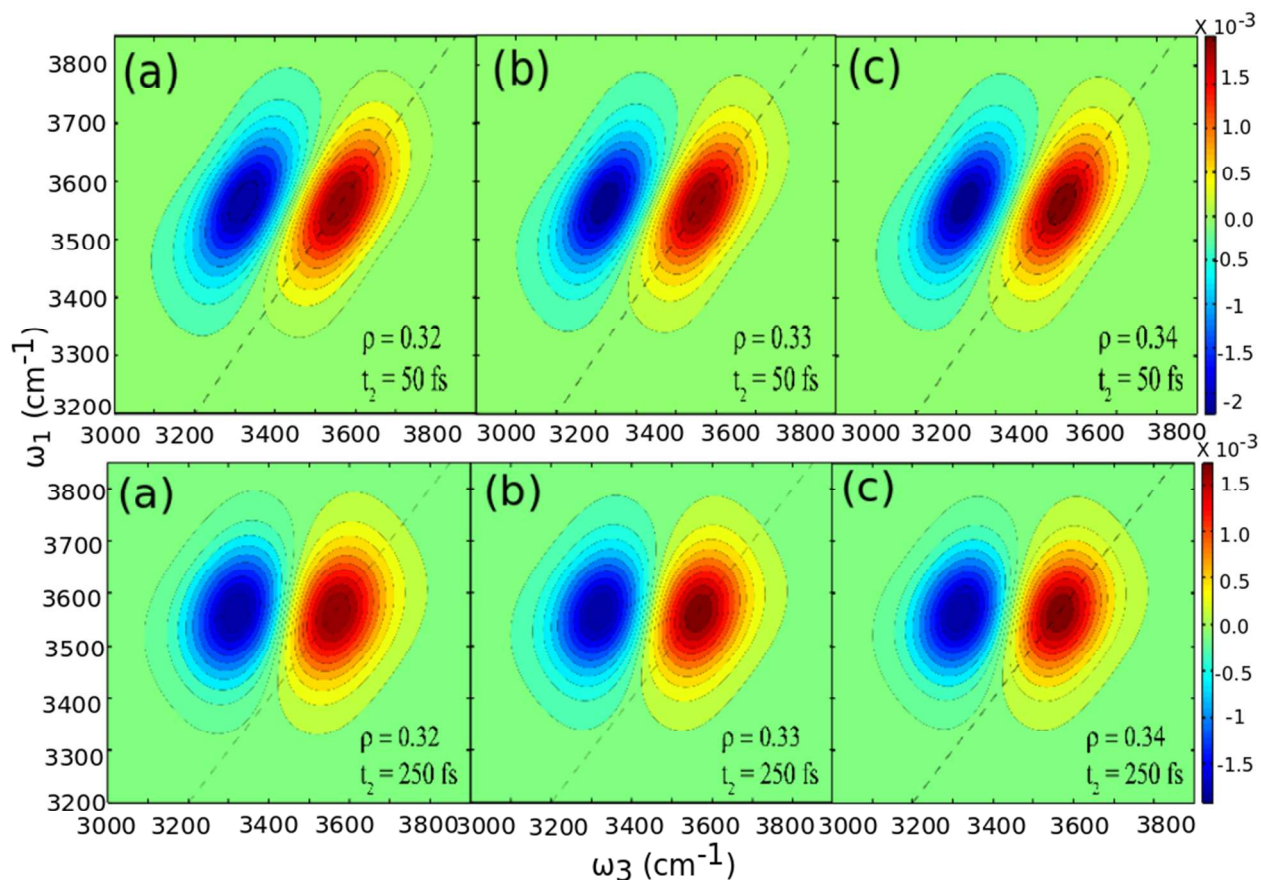
Figure 5. 2D – IR spectra for different densities (a) $\rho = 0.32 gm/cm^3$ (b) $\rho = 0.33 gm/cm^3$ (c) $\rho = 0.34 gm/cm^{3,}$ with delay time $t_2 = 50$ fs (upper panel) and 250 fs (lower panel). Note that at short time for all densities the inhomogeneous environments of system are well captured by the diagonal elongation of 2D IR spectra, at temperature 670 K.

Using the same technique as describe above, we plot 2D-IR spectra of the -O-H stretch for super critical water measured at different waiting times (**Figure 5**). Due to vibrational anharmonicity the red and blue bands are shifted toward lower values of the ω_3 axis. The spectra with short delay time (50 fs) show a pronounced diagonal elongation, arising due to incomplete spectral diffusion and inhomogeneous broadening. However, increase in the waiting time causes the -O-H bond to start sampling an average environment that is homogenous in nature and thereby leads to complete spectral diffusion. For a larger waiting time we expect to

get a symmetric shape of the 2D-IR spectra. The observed 2D-IR spectra reflect the enhanced inhomogeneity in the vicinity of the critical point ($(\rho \sim 0.33 gm/cm^3)$. This essentially gives a slower spectral diffusion. However such spectral diffusion is relatively faster for other densities.

We establish an idea about the time-scale of the heterogeneity by plotting dynamical four point susceptibility, $\chi_4(t)$. $\chi_4(t)$ essentially measures the spatio-temporal correlation between the local density at two points in space at two different times. Thus, as the critical point is approached and system becomes intrinsically more heterogeneous, $\chi_4(t)$ is generally found to be increasingly more pronounced.
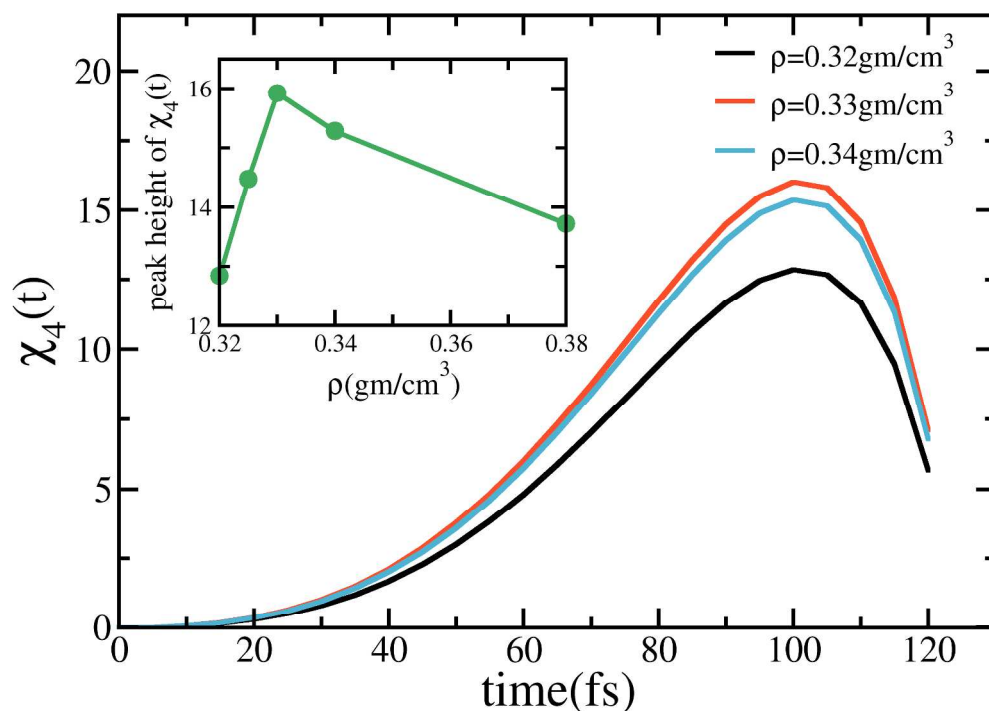
Figure 6. Four point density susceptibility versus time for different average densities at 670K. In the inset, the respective peak maxima of four point susceptibility are plotted with density, all at T=670K. Note that the inset plot, density dependent peak height of four point susceptibility shows a maximum at ρ = 0.33 gm/cm³.

In **Figure 6** we plot $\chi_4(t)$ for the density range of 0.32-0.34 gm/cm^3 (around critical density) at

T=670K . For all densities, $\chi_4(t)$ is nearly zero at short time and peaks at around 100 fs. This

essentially suggests that dynamic heterogeneity present in SCW has a lifetime of the order of 100

fs. The variation of peak height of $\chi_4(t)$ with density is shown in the inset of **Figure 6**. The peak

height shows a maximum at the density (ρ) 0.33 gm/cm^3, as expected. As we go beyond the

density (ρ) 0.33 gm/cm^3 the peak height value of $\chi_4(t)$ again decreases. It signifies the system

becomes more homogeneous as we move away from critical point.
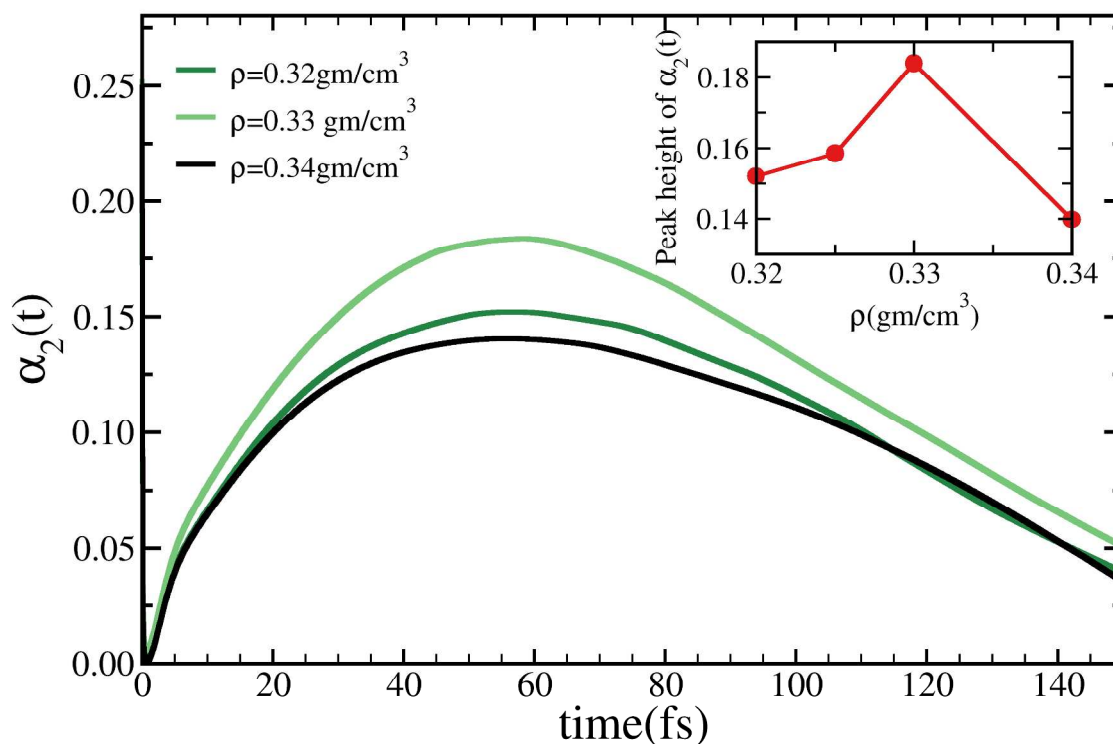
Figure 7. Temporal evolution of the non-Gaussian parameter for different densities (inset: variation of peak maxima of non-Gaussian parameter along with varying density). Note that the inset plot shows a transition of peak maximum again at $\rho = 0.33$ gm/cm^3 where non-Gaussian behavior and heterogeneity are maximum.

18

The well-known non-Gaussian parameter $\alpha_2(t)$ demonstrates the presence of static heterogeneity in a system. It is not sensitive to dynamic heterogeneity and therefore a comparison between $\chi_4(t)$ and $\alpha_2(t)$ provides a useful way to separate static heterogeneity from dynamic heterogeneity.

In **Figure 7**, we observe large value of $\alpha_2(t)$ due to presence of long lived heterogeneity near critical density ($\rho_c = 0.33$ gm/cm^3). Deviation from the Gaussian behavior becomes less prominent in all densities except that of critical density. The time scale of static heterogeneity is found to be prevailing at around ~ 70 fs (as observed from the peak position).

V.   Spatio-temporal resolution of polarization fluctuations in aqueous protein solutions

Aqueous protein solutions serve as an important subject of study, as the large dipole moment of the protein molecules can significantly perturb dynamics of water molecules. One of the most relevant properties that is anticipated to be affected due to presence of such large dipoles, is the collective polarization fluctuation, related to the dielectric constant of the solution.

In this particular problem we have not yet been able to generate the 2D-IR spectra at different layers. The difficulty is to account for the effects of all the atoms of the protein on the spectral diffusion of –O-H vibrational mode. Even the calculation of the average frequency within the Condon approximation is a non-trivial (but not an impossible) task. We leave this work for future. But we can obtain some degree of information from study of various time correlation function, particularly from the comparison of water dynamics for the two different proteins.

We explore these aspects by studying aqueous solutions of two different proteins, immunoglobulin binding domain protein G (GB1) and hen-egg white lysozyme (LYS) of different characteristics (shown in **Figure 8**). We find that the calculated dielectric constant of the system shows a noticeable increment in all the cases compared to that of neat water (for SPC/E model water the estimated value is ~ 68). Total dipole moment auto time correlation function of water $\langle \delta M_W(0)\delta M_W(t)\rangle$ is found to be sensitive to the nature of the protein. A shell-wise decomposition of water molecules around protein reveals higher density of first layer compared to the succeeding ones.

(a)   (b)
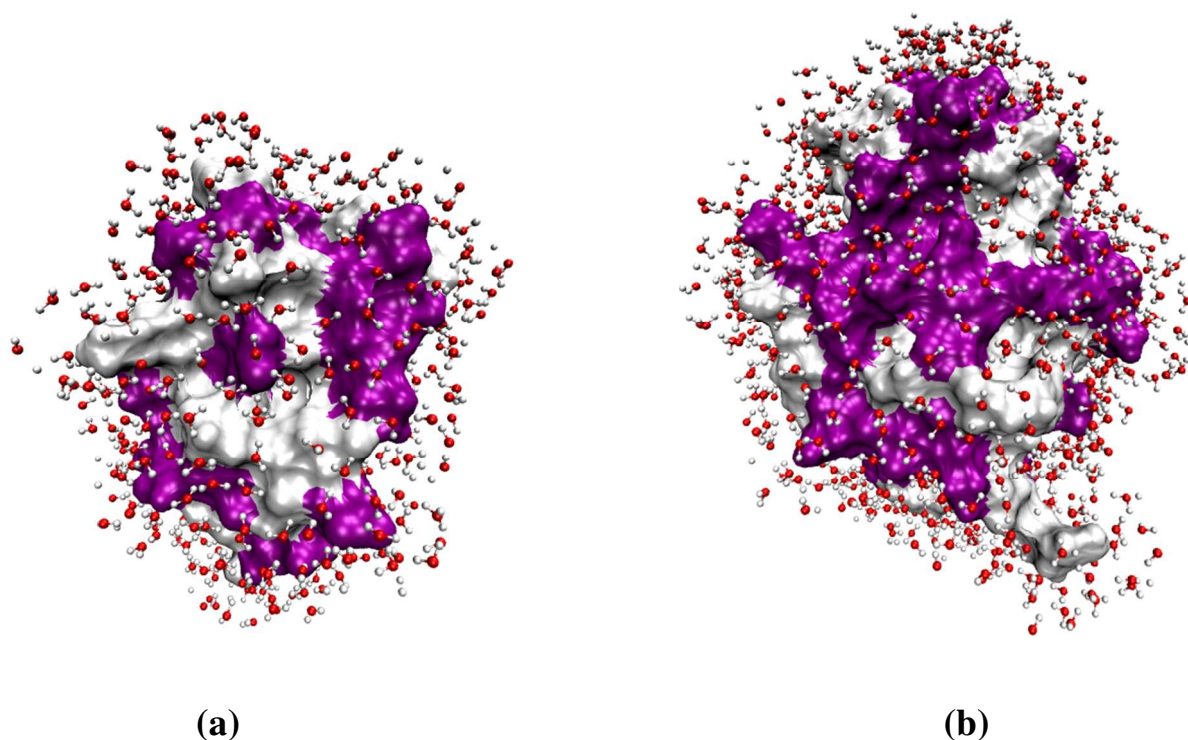
Figure 8. Representative conformational surface of the two proteins investigated in this work- (a) protein G (56 residues) (b) lysozyme (129 residues). Purple surface represents the hydrophilic patch whereas white surface represents the hydrophobic patch. Water layer around the protein up to 5 Å is shown. Note that the two proteins are quite different.

A. Simulation Details

We have performed atomistic molecular dynamics simulation of the two proteins with sufficiently large number of water molecules (number varied according to size of the proteins) and at 300K temperature and 1 bar pressure. For protein G (PDB ID: GB1) we have used ~8.5 nm box and 20893 water molecules and for lysozyme (PDB ID: 1AKI) we have used ~9.5 nm box and 29204 water molecules. We have used OPLS-AA[25] force field and extended simple point charge model (SPC/E)[26] for water. After performing steepest descent energy minimization, the solvent was further equilibrated for 10 ns by restraining the position of protein. Finally production run was performed for 20 ns in NPT ensemble. Temperature was kept constant using Nose-Hoover[21,22] Thermostat and Parrinello-Rahman Barostat[23] was used for pressure coupling. After final equilibration of the system, a further 5 ns run was performed with 10 fs resolution to generate trajectory for calculating the correlation functions.

B. Evaluation of total and local polarization fluctuation of water in aqueous protein solutions

In **Figure 9**. we plot the correlation in the fluctuation of total dipole moment of water $\langle \delta M_W(0) \delta M_W(t) \rangle$ for the two proteins. The detailed nature of the correlation functions is expected to be sensitive to the protein size, amino acid sequence as well as orientation of corresponding dipoles. Whereas the correlation functions are decaying within 80 ps for lysozyme, in case of GB1 the decay is found to be comparatively faster and reaching 0 within 40 ps. The correlation functions are fitted to exponential forms and the corresponding amplitudes

and time constants are given in **Table 3**. We find that the corresponding correlation function for

GB1 fits to a single exponential form with a time constant of 10.9 ps that is a signature of the fast

water. However lysozyme fits to a bi-exponential with two time constants; first time constant

signifies fast dynamics of free water and the second time constant is a signature of slow

biological water. Interestingly, in both the cases we find that the estimated value of dielectric

constant of water is higher than the normal value (for SPC/E water, dielectric constant is ~ 68).

Protein	**a$_1$**	τ_1 (ps)	**a$_2$**	τ_2 (ps)	ε
GB1	0.97	10.9	-	-	75.4
LYS	0.749	6.9	0.251	31.7	70.9
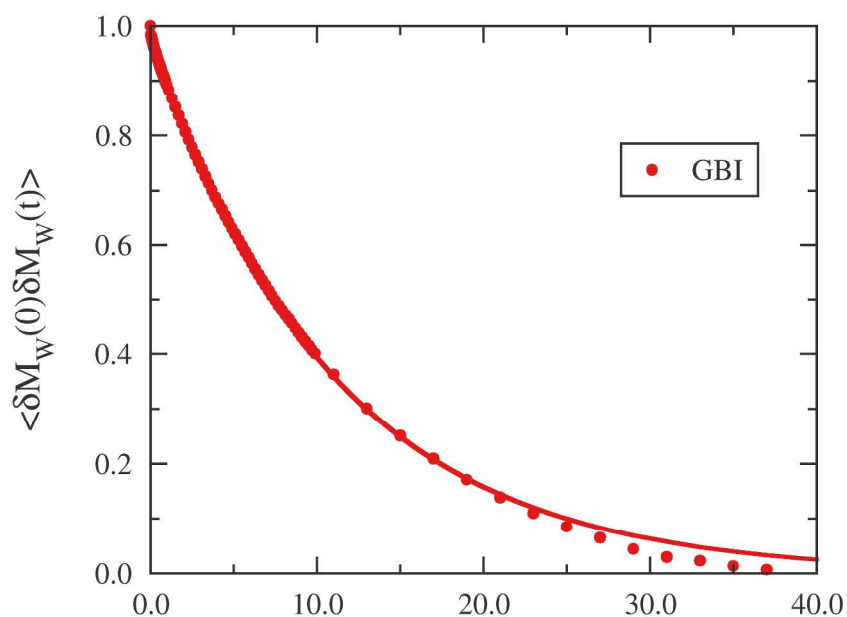
(a)
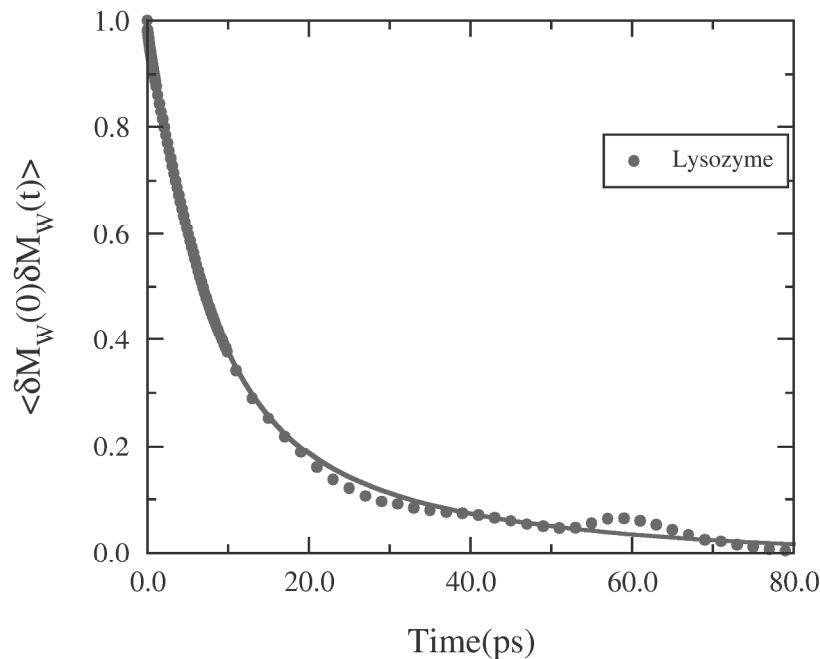
(b)

Figure 9. Dipole-dipole auto-correlation functions of water $\left\langle \delta M_W(0)\delta M_W(t) \right\rangle$ **for (a) Protein G**

(GB1) (b) Lysozyme (Lys). In both the cases the correlation is found to decay to zero within 100 ps.

In **Figure 10** we show shell-wise decomposition of the partial dipole moment-dipole moment

time correlation function $\left\langle \delta M_i(0)\delta M_i(t) \right\rangle$ (i – shell index) for the first two shells (shells are

taken to be approximately ~ 1 nm thick). For lysozyme striking observation is the considerable

slowing down of polarization fluctuation for the first shell. By second shell, relaxation achieves

almost bulk-like behavior. However GB1 protein shows bulk like decay even for the first shell.

The slowing down of relaxation for lysozyme in the first shell emerges due to the appearance of

an additional relaxation channel in the relaxation of biological water that is found to be missing

in case of GB1. The associated slow relaxation time is of the order of 40 ps. Surprisingly, shell-

wise calculation of dielectric constant gives much lower value for the both the shells (first shell: 49.2 for GB1 and 48.31 for lysozyme; second shell: 59.3 for GB1 and 53.3 for lysozyme) compared to that of bulk.
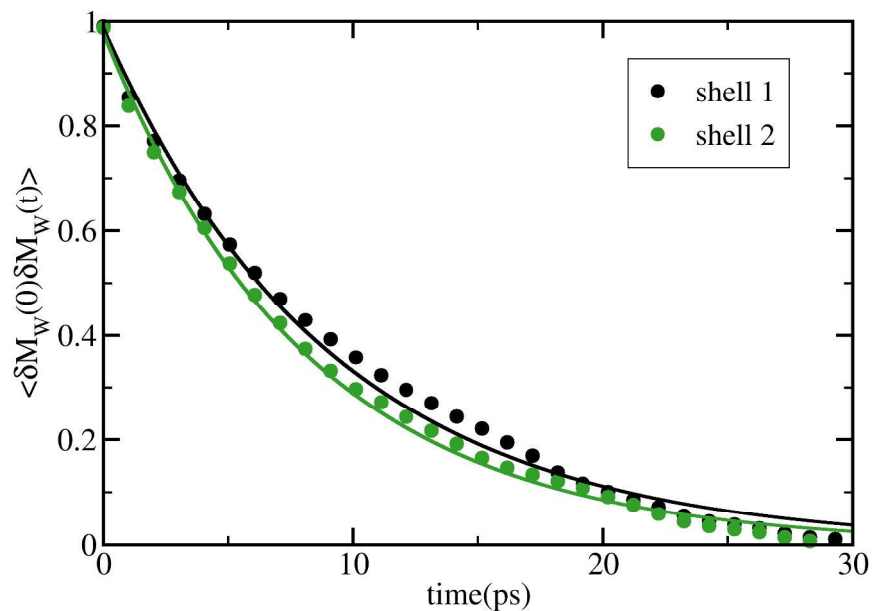
(a)
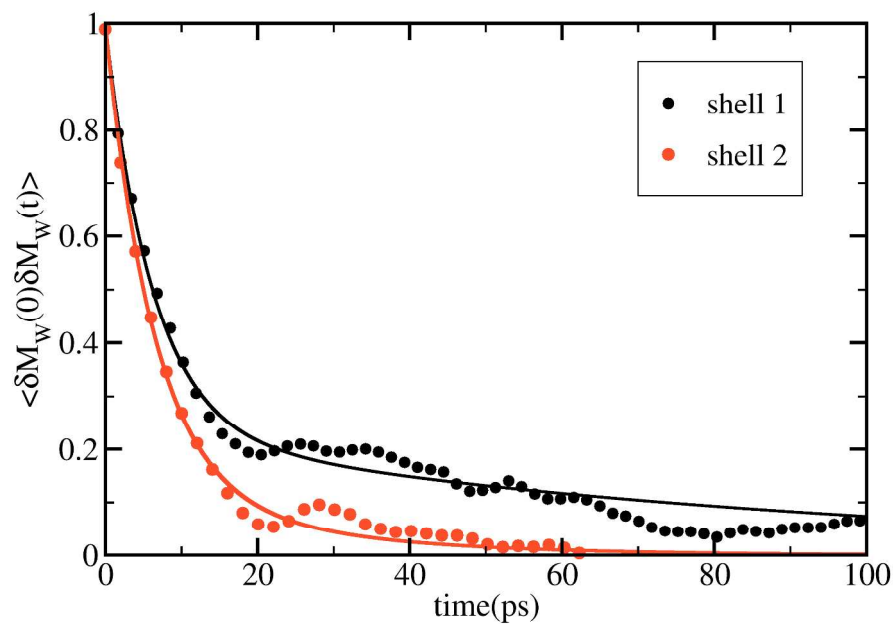
(b)

Figure 6. Demonstration of shell-wise polarization fluctuation of water for (a) GB1 (b) Lysozyme.

VI.   Conclusion

Omnipresence of heterogeneity in natural aqueous systems has always been an intriguing subject of study. The heterogeneity is mostly local, a few molecular layers thick and lead to unusual dynamics. In this work we explore the consequences (both spatial and temporal) of heterogeneity in different aqueous systems. In all the cases, we find that the heterogeneity is reflected through significant alteration of water dynamics. In the case of reverse micelle, we find that with increasing system size, the dynamical behavior of water in different layers varies substantially. Thermodynamics induced heterogeneity in super critical water is also well reflected in the corresponding spectral diffusion of 2D-IR spectra. Here the time scales of density relaxation are ultrafast and captured faithfully by 2D-IR spectra. Finally, we evaluate local and collective polarization fluctuation in aqueous protein solutions, where we also find prominent signature of heterogeneity. The present work is thus successful in identifying and generalizing the existence of heterogeneity in various aqueous systems.

 In future we plan to calculate 2D-IR spectra of aqueous the –O-H mode in different hydration layers of protein solutions.

VII. References

†Electronic Supplementary Information (ESI) available: [figures showing layerwise calculation of frequency fluctuation correlation functions with increasing reverse micelle size, and comparison with that of bulk]. See DOI:

(1)   Bagchi, B.: *Water in Biological and Chemical Processes: From Structure and Dynamics to Function*; Cambridge University Press, 2014.

(2)   Fayer, M. D.; Levinger, N. E.: Analysis of Water in Confined Geometries and at Interfaces. *Annual Review of Analytical Chemistry* **2010**, *3*, 89-107.

(3)   Pal, S. K.; Zewail, A. H.: Dynamics of Water in Biological Recognition. *Chemical Reviews* **2004**, *104*, 2099-2124.

(4)   Nandi, N.; Bagchi, B.: Dielectric Relaxation of Biological Water†. *The Journal of Physical Chemistry B* **1997**, *101*, 10954-10961.

(5)   Telgmann, T.; Kaatze, U.: On the Kinetics of the Formation of Small Micelles. 1. Broadband Ultrasonic Absorption Spectrometry. *The Journal of Physical Chemistry B* **1997**, *101*, 7758-7765.

(6)   Ladanyi, B. M.: Computer simulation studies of counterion effects on the properties of surfactant systems. *Current Opinion in Colloid & Interface Science* **2013**, *18*, 15-25.

(7)   Vajda, S.; Jimenez, R.; Rosenthal, S. J.; Fidler, V.; Fleming, G. R.; Castner, E. W.: Femtosecond to nanosecond solvation dynamics in pure water and inside the [gamma]-cyclodextrin cavity. *Journal of the Chemical Society, Faraday Transactions* **1995**, *91*, 867-873.

(8)   Tucker, S. C.: Solvent Density Inhomogeneities in Supercritical Fluids. *Chemical Reviews* **1999**, *99*, 391-418.

(9)   Bagchi, B.: Water Dynamics in the Hydration Layer around Proteins and Micelles. *Chemical Reviews* **2005**, *105*, 3197-3219.

(10)   Biswas, R.; Furtado, J.; Bagchi, B.: Layerwise decomposition of water dynamics in reverse micelles: A simulation study of two-dimensional infrared spectrum. *The Journal of Chemical Physics* **2013**, *139*, -.

(11)   Pronk, S.; Lindahl, E.; Kasson, P. M.: Dynamic heterogeneity controls diffusion and viscosity near biological interfaces. *Nat Commun* **2014**, *5*.

(12)   Zanni, M. T.; Hochstrasser, R. M.: Two-dimensional infrared spectroscopy: a promising new method for the time resolution of structures. *Current Opinion in Structural Biology* **2001**, *11*, 516-522.

(13)   Zheng, J.; Kwak, K.; Fayer, M. D.: Ultrafast 2D IR Vibrational Echo Spectroscopy. *Accounts of Chemical Research* **2006**, *40*, 75-83.

(14)   Hamm, P.; Zanni, M.: *Concepts and Methods of 2D Infrared Spectroscopy*; Cambridge University Press, 2011.

(15)   Roberts, S. T.; Ramasesha, K.; Tokmakoff, A.: Structural Rearrangements in Water Viewed Through Two-Dimensional Infrared Spectroscopy. *Accounts of Chemical Research* **2009**, *42*, 1239-1249.

(16)   Nandi, N.; Bagchi, B.: Anomalous Dielectric Relaxation of Aqueous Protein Solutions. *The Journal of Physical Chemistry A* **1998**, *102*, 8217-8221.

(17)   Pethig, R.: Protein-Water Interactions Determined by Dielectric Methods. *Annual Review of Physical Chemistry* **1992**, *43*, 177-205.

(18)   Nandi, N.; Bhattacharyya, K.; Bagchi, B.: Dielectric Relaxation and Solvation Dynamics of Water in Complex Chemical and Biological Systems. *Chemical Reviews* **2000**, *100*, 2013-2046.

(19)   Abascal, J. L. F.; Vega, C.: A general purpose model for the condensed phases of water: TIP4P/2005. *The Journal of Chemical Physics* **2005**, *123*, -.

(20)   Hess, B.; Kutzner, C.; van der Spoel, D.; Lindahl, E.: GROMACS 4: Algorithms for Highly Efficient, Load-Balanced, and Scalable Molecular Simulation. *Journal of Chemical Theory and Computation* **2008**, *4*, 435-447.

(21)   Nosé, S.: A unified formulation of the constant temperature molecular dynamics methods. *The Journal of Chemical Physics* **1984**, *81*, 511-519.

(22)   Hoover, W. G.: Canonical dynamics: Equilibrium phase-space distributions. *Physical Review A* **1985**, *31*, 1695-1697.

(23)   Parrinello, M.; Rahman, A.: Polymorphic transitions in single crystals: A new molecular dynamics method. *Journal of Applied Physics* **1981**, *52*, 7182-7190.

(24)   Roychowdhury, S.; Bagchi, B.: Vibrational phase relaxation of O–H stretch in bulk water: Role of large amplitude angular jumps and negative cross-correlations among the forces on the O–H bond. *Chemical Physics* **2008**, *343*, 76-82.

(25)   Jorgensen, W. L.; Maxwell, D. S.; Tirado-Rives, J.: Development and Testing of the OPLS All-Atom Force Field on Conformational Energetics and Properties of Organic Liquids. *Journal of the American Chemical Society* **1996**, *118*, 11225-11236.

(26)   Berendsen, H. J. C.; Grigera, J. R.; Straatsma, T. P.: The missing term in effective pair potentials. *The Journal of Physical Chemistry* **1987**, *91*, 6269-6271.